Journal of Alloys and Compounds 790 (2019) 1043–1050

Contents lists available at ScienceDirect

Journal of Alloys and Compounds

journal homepage: http://www.elsevier.com/locate/jalcom

Sn accommodation in tunable-void and porous graphene bumper for high-performance Li- and Na-ion storage

Xiaoxu Liu [a], Na Li [c], Chen Yang [c], Zhen Liu [d], Yanqi Feng [a], Wanmeng Dong [a], Shikun Liu [b], Hui Liu [a], Yanlin Jia [e, f, *], Jiupeng Zhao [b, **], Yao Li [b, g, ***]

[a] School of Material Science and Engineering, Shaanxi Key Laboratory of Green Preparation and Functionalization for Inorganic Materials,Shaanxi University of Science and Technology, Xi'an, 710021, China
[b] School of Chemical Engineering and Technology, Harbin Institute of Technology, Harbin, 150001, China
[c] Heilongjiang University of Science and Technology, Harbin 150027, China
[d] Institute of Electrochemistry, Clausthal University of Technology, Arnold-Sommerfeld-Strasse 6, 38678 Clausthal-Zellerfeld, Germany
[e] College of Materials Science and Engineering, Central South University, Changsha, 410083, China
[f] College of Materials Science and Engineering, Beijing University of Technology, Chaoyang District, Beijing 100124, China
[g] Center for Composite Materials, Harbin Institute of Technology, Harbin, 150001, China

ARTICLE INFO

Article history:
Received 16 February 2019
Received in revised form
17 March 2019
Accepted 18 March 2019
Available online 19 March 2019

Keywords:
Sn anode
3D Porous
graphene
High-performance
Lithium ion battery
Na-ion storage

ABSTRACT

Nanoscale microstructure designing is playing an important role in improving the performance of electrode materials of an electrochemical battery. The Sn based anode is among the very high-capacity but less-stable materials, and has been used mostly for anode of the Li-ion battery with unsatisfactory performance. In this work, we design a new type of 3D porous graphene and nano-Sn composite (Sn/Void@G) by simple one-step annealing of graphene oxide, polystyrene spheres and stannic chloride for both high performance Li- and Na-ion battery anodes. More importantly, the 3D porous graphene formed tunable micro-nano void as a highly efficient "bumper" to accommodate the large volume expansion of nano-Sn particles. As results, the discharge specific capacity of the Sn/Void@G, anode still remains 45.3% while the charge-discharge current is increased 50 times, and the capacity is more than 400 mAh g^{-1} after 500 cycles at 5C rate. For Na storage, the integrated anodes deliver the Na storage capacity of 786.1 mAh/g at 0.1C rate and the capacity of more than 340 mAh/g after 800 cycles at 2C rate. The present result on Li and Na ion battery may pave the way to next generation high power and energy density batteries.

© 2019 Elsevier B.V. All rights reserved.

1. Introduction

In the past decades, Lithium-ion batteries (LIBs) and Sodium-ion batteries (SIBs) [1–4], as electrical energy storages, have been widely used in portable electronic devices [5–8]. However, the increasing demand for their emerging applications in electric vehicles and large-scale energy storage requires us to enhance its energy and power density. As we know, electrode materials play a crucial role in the battery performance. Thus, higher specific capacity and longer cycling life anodes, which are important factors for the battery performance, need to be developed while commercial graphite anode (theoretical capacity for LIBs: 372 mAh g^{-1}) is reaching the energy and power limitation. Because of their higher theoretical capacity, many metals have been intensively studied as anodic electrodes for the next-generation LIBs, such as Ge [9], Si [10], Sn [11]. Thanks to the advantages of a high theoretical specific capacity (993 mAh g^{-1}), low cost, abundance in nature, and environmental friendliness, Sn has been considered as one of the promising anode candidates [12,13]. However, the large volume change results in severe mechanical damage of Sn-based electrodes and subsequently leads to rapid capacity fading during the repetitive discharge/charge process [14,15].

In order to overcome the challenges thereof, two main effective methods have been reported in research. One approach is to reduce the particle size of Sn to the nanoscale to alleviate the large volume

* Corresponding author. College of Materials Science and Engineering, Central South University, Changsha, 410083, China.
** Corresponding author.
*** Corresponding author. School of Chemical Engineering and Technology, Harbin Institute of Technology, Harbin, 150001, China.
E-mail addresses: jiayanlin@126.com (Y. Jia), jpzhao@hit.edu.cn (J. Zhao), yaoli@hit.edu.cn (Y. Li).

https://doi.org/10.1016/j.jallcom.2019.03.258
0925-8388/© 2019 Elsevier B.V. All rights reserved.

change [16–19]. However, nanosized Sn particles prefer aggregating during the cycling, resulting in rapid capacity fading [20]. Another way is to integrate Sn nanoparticles with a conductive carbon matrix [21], which can mitigate the mechanical stress and accommodate the volume variation. So far, various carbon matrices have been applied [22–33], such as mesoporous carbon [20], amorphous carbon [34], graphite [35], carbon nanotubes [36], and carbon nanofibers [37].

In this study, we reported a novel 3D porous reduced graphene and nano-Sn composite (Sn/Void@G) electrode through a facile template strategy involving a self-assembly process of graphene sheets (in nickel foam using stannic chloride, graphene oxide, polystyrene spheres as precursors), removal of polystyrene spheres (PS) template, thermal activation, and carbothermal reduced Sn^{+4} into Sn nanoparticles. The Sn/Void@G electrodes possess a hierarchically porous structure for being of the macro-porous architecture of Ni foam, and porous reduced graphene, which could effectively improve the mechanical strength and provide sufficient contact areas between the Sn/Void@G electrode and electrolyte. The prepared Sn/Void@G electrode exhibits a relatively good reversible specific capacity, an excellent rate capability, and durable cycling stability for both Li and Na ion batteries, because of their hierarchical three-dimensional architecture and expansible graphene interlayer distance. This unique micro-/nanostructures are beneficial to achieve high energy and power densities. For example, the Sn/Void@G as LIB anode exhibited the reversible specific capacity of 868.9 mA h g^{-1} at 0.1C rate. Its discharge specific capacity still remained 45.3% when the charge-discharge current increased to 50 times higher and the first coulomb efficiency was 62.5% and then ~99.6% in the following cycles. Moreover, a sodium storage capacity of 786.1 mAh g^{-1} was obtained when it was used as electrode for SIB at 0.1C rate. A specific capacity as high as 166 mAh g^{-1} can be achieved at 20C, and no obvious capacity fading was observed after more than 800 cycles of continuous charge/discharge at 2C rate. Furthermore, the synthesized Sn/Void@G electrode avoids the addition of binder and conductive additives and thus could be more beneficial to a large-scale application.

2. Experimental details

2.1. Preparation of composite electrodes

Nickel foam (110PPI, 420 g/cm^2, thickness 1.4 mm) was first cut into electrode wafers with a diameter of 1.5 cm and then washed with ethanol several times. The pre-treated Ni foam wafers were immersed into n-methyl-2-pyrrolidone containing polyaniline (0.025 wt %) several hours. In a representative preparation process, 27.4 mg $SnCl_4 \cdot 2H_2O$ (Sinopharm Chemical Reagent Co., Ltd.) was first dissolved in 4 mL deionized (DI) water and then graphene oxide (1 mL, 9.3 g/mL) and polystyrene spheres (3 mL, 380 nm, 10.97 wt%) were added into the solution under magnetic stirring. The preparation of graphene oxide can be found in the Supporting information. The gray mixture was continuously sonicated and magnetically stirred to form a homogeneous suspension. The pre-treated Ni foam wafers were immersed in the precursor solution, and then dried in a dry oven at 60 °C. The dry samples embedded in the nickel foam wafers were calcinated in Ar at 200 °C for 1 h and then at 800 °C for 2 h, while the Sn^{4+} was converted to metallic Sn via a carbothermal reduction step [38]. Eventually, the final products, the Sn/Void@G electrode, were ready to directly serve as the anode of LIBs and SIBs.

2.2. Characterization

X-ray diffraction (XRD) analysis was performed with a Rigaku RU-200BVH diffractometer employing a Cu-K α source. The diffraction patterns were collected at room temperature in the 2θ ranges of 10–90°. Scanning electron microscopy (SEM) was conducted using a Hitachi S-4800 scanning electron microscope operating at 15 kV. Transmission electron microscopy (TEM) images were taken with a JEOL2010F at an acceleration voltage of 20 kV. X-ray photoelectron spectroscopy (XPS) measurements were performed on a PHI 5400 ESCA System Al at 1486.6 eV. Raman spectra were collected using a 532 nm laser in a WITec CRM 200 confocal.

2.3. Electrochemical measurements

The electrochemical properties of the Sn/Void@G electrodes were measured using two-electrode CR2032 (3 V) coin-type cells. The half cell assembled in an argon-filled glovebox (Vigor Glove Box from Suzhou, China) with water and oxygen contents of below 1.0 ppm. Lithium sheets were used as the counter electrode and reference electrode with a polypropylene (PP) film (Cellgard 2400) as the separator. The electrolyte was 1 M $LiPF_6$ in ethylene carbonate (EC)-dimethyl carbonate (DMC) (1:1 in volume), without any additives. The Sn/Void@G electrodes were directly used as the anode. The galvanostatic charge-discharge property of the batteries was examined using a channels battery analyzer (NEWARE CT3008, China) at a voltage window between 0.01 and 3.0 V (vs. Li^+/Li). For sodium ion battery fabrication, metallic Na foil was used as the counter/reference electrode, glass fiber (Whatman) was used as the separator, and 1 M $NaClO_4$ in ethylene carbonate (EC)-diethyl carbonate (DEC) (1:1 in volume) was used as the electrolyte. The discharge-charge performance of the batteries was tested using a battery analyzer (Neware CT-3008) with the voltage cut-off between 0 and 3.0 V vs. Na/Na^+. The electrochemical impedance spectroscopy (EIS) and cyclic voltammetry (CV) measurements were performed using a CHI660E electrochemical workstation. EIS was recorded with a frequency ranging from 100 kHz to 10 mHz and an AC signal of 5 mV in amplitude as the perturbation. The voltage range of the CV measurements was 0–3.0 V and the scanning rate was 0.5 mV s^{-1}. All the tests were performed and measured at room temperature.

3. Results and discussions

A schematic illustration of the general preparation process for the Sn/Void@G electrode is depicted in Fig. 1. The first step of the fabrication process is pre-treating nickel foam. Nickel foam is cut into electrode wafers and washed with ethanol several times, then immersed in n-methyl-2-pyrrolidone containing polyaniline several hours. The second step is to impregnate the pre-treated nickel foam wafers with the precursor solution containing GO, PS, and $SnCl_4 \cdot 2H_2O$. The water in the precursor composite is removed from the surface of Ni foam with a dry oven. Finally, the Sn/Void@G electrodes are obtained by claiming the dried nickel foam wafers coating precursor composite in Ar atmosphere, where PS spheres are decomposed and leaving lots of sphere-like voids (Fig. 1). Furthermore, a precursor composite of dried GO was in situ reduced, and the tin ion is oxidized without any auxiliary reagents. As a result, Sn particles are embedded between graphene sheets on pore wall of 3D porous structure at the same time.

The morphology of Sn/Void@G-800 electrode (After impregnating with the precursor solution and annealing at 800 °C) is shown in Fig. 2a and Figs. S1a and a visible black carbon coating layer can be found on the whole nickel foam skeletons uniformly. The macroporous structure form can be obviously observed from high-magnification SEM images (Fig. 2b and Fig. S2b). The inner surface of macropores is rough and the pore walls are composed of graphene sheets with embedded Sn nanoparticles. Due to the

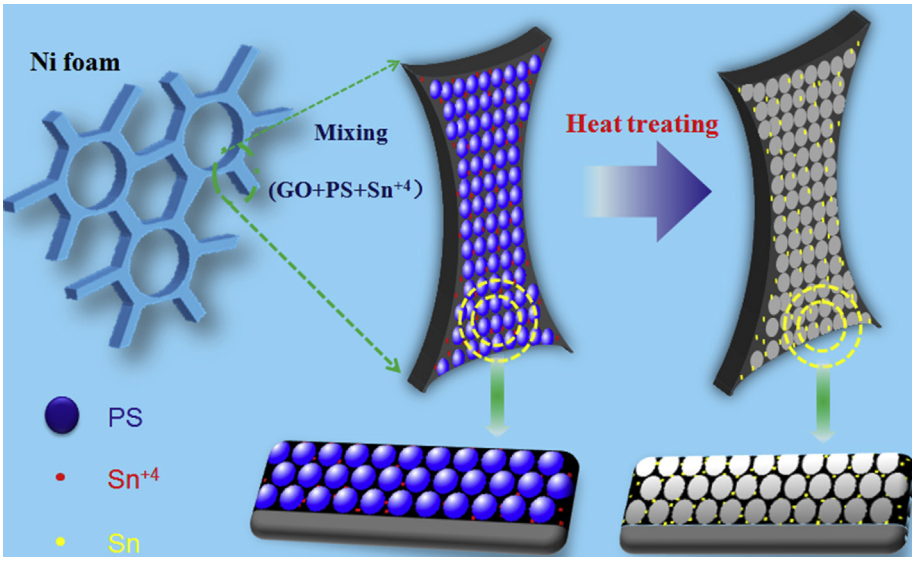

Fig. 1. Schematics illustration for the fabrication of the Sn/VOID@G electrodes.

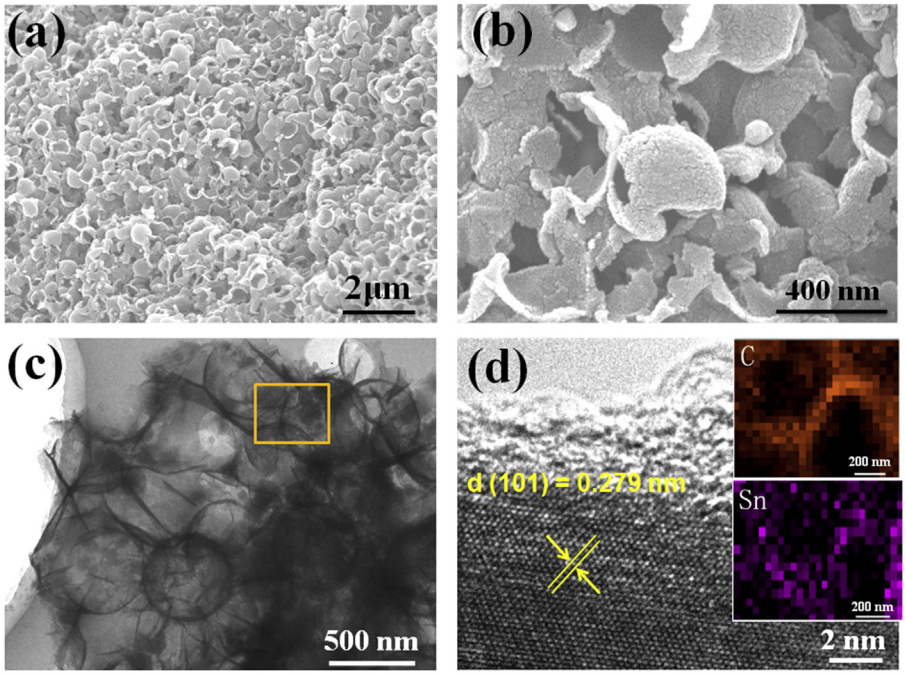

Fig. 2. (a–b) SEM images of the Sn/Void@G-800 sample; (c) TEM image of the Sn/Void @G-800 samples; (d) HRTEM images of the Sn/Void @G-800 sample; inset images for the elemental mapping images of C and Sn elements in the Sn/Void @G-800 sample.

existence of the graphene porous microstructure of on the Sn/Void@G-800 electrode, the hydrophobic performance of the Sn/Void@G-800 electrode is observably improved compared with the original nickel foam in Figs. S1b and c (the morphology of original nickel foam is shown in the low-magnification SEM image of Fig. S2a). Besides, Fig. 2c reveals that the average diameter of individual macropores is approximate 400 nm, which is in agreement with the size of PS precursor template. Obviously, the nano architecture enables the Sn/Void@G-800 electrode to possess high surface electrochemical reactivity, and the high hydrophobic macroporous structure is effective for the infiltration of the organic electrolyte [39]. In order to further proving the formation mechanism of the porous structure, the different annealing temperature has been controlled. At 600 °C annealing, the 3D interconnected porous graphene frameworks with Sn particle (named Sn/Void@G-600) were also formed. This means that the formation of 3D interconnected porous structure is due to the pyrolysis of PS templates, so the size of nanospheres making up a 3D porous microsphere could be easily manipulated by controlling the PS sphere size. When the size of PS template is larger than 500 nm, obtained 3D porous structure of Sn/Void@G is more easily broken. However, when the size of PS template is less than 300 nm, the 3D structure gets more irregular (see Figs. S3 and S4). Some typical TEM and HRTEM images of the Sn/Void@G-800 sample further exhibited in Fig. 2c–d. It was further proved that the wrinkled graphene sheets form the 3D interconnected porous structures, and the Sn particles

with the average particle size less than 100 nm are homogeneously dispersed on surface of the graphene matrix (in Fig. 2c). Meanwhile, the HRTEM images reveal that the interplanar distances of 0.279 nm can be viewed as d (101) of crystal Sn (see Fig. 2d). An elemental mapping of Sn/Void@G-800 sample by energy-dispersive X-ray spectroscopy (EDS) analysis is shown in inset images of Fig. 2d. It verifies that the Sn nanoparticles are embedded in the filmy graphene sheets.

The crystal structures and phases of various samples can be further investigated by XRD [40], Raman and XPS spectroscopy. The XRD patterns of Sn/Void@G-800, in good agreement with reported data (JCPDS no. 04-0673), shows three strong diffraction peaks at 30.6°, 32.0°and 44.9°, which are corresponding to (200), (101) and (211) crystal planes of Sn respectively (see Fig. 3a). For the Sn/Void@G-800 sample, the diffraction peak at $2\theta = 32.0°$ is attributed to the (101) crystal plane of Sn nanoparticle, which agrees with lattice spacing 0.279 nm in the HRTEM of Fig. 2d, and no peaks of impurities were found, indicating the Sn^{4+} are completely converted to crystalline Sn nanoparticle. The Sn/Void@G-800 samples have been also characterized by Raman spectroscopy in Fig. 3b, and the spectrum exhibit two characteristic peaks of graphene, at 1337 and 1590 cm^{-1}, which are corresponding to the D and G bands. The peak at approximately 1590 cm^{-1} (G-band) is due to the in-plane vibrations of sp^2-bonded carbon atoms. Moreover, a peak at approximately 1337 cm^{-1} (D-band) is due to the presence of vacancies, grain boundaries and amorphous carbon species [41]. Meanwhile, the Raman peaks at ~2700 of sample is second order D band for identifying second order vibrational mode. The intensity ratio (I_D/I_G) associates with the size and disorder degree of sp2 domains [42]. From the intensity ratio of the data, the I_D is lower than I_G, revealing that higher temperature can decrease the disorder degree. The wide angle XPS of Sn/Void@G-800 shows that the peaks of C, Sn, Ni and O are predominant signals in the general survey spectrum (see Fig. S5). The peak of Ni is due to the presence of nickel foams. In the C 1s spectra of Sn/Void @G-800, four peaks centered at 284.6, 285.5, 287.6 and 289.0 eV appear, generally assigned to C-C, C-OH, C-O and C═O, respectively (see Fig. 3c) [43]. Additionally, the spin energy separation of Sn $3d_{5/2}$ and Sn $3d_{3/2}$ centered at the binding energies of 485.1 and 493.5 eV, respectively, which is in well agreement with reported data for Sn element (see Fig. 3d), indicating the Sn in the Sn/Void @G-800 composite [44–48].

The electrochemical storage Li performance of the Sn/Void@G as the anode of lithium ion battery (LIBs) was investigated. Fig. 4a shows the first five galvanostatic charge-discharge profiles of Sn/Void@G. The initial discharge/charge capacities of Sn/Void@G-800 are 1390.8 mA h g^{-1} and 868.9 mA h g^{-1} with initial coulombic efficiency of 62.5%. The Sn/Void@G-800 anode has a higher reversible capacities and initial coulombic efficiency than Sn/Void@G-600 anode (see Fig. S6). The cyclic voltammograms (CVs) of the Sn/Void@G-800 and Sn/Void@G-600 electrodes shown in Fig. 4b and Fig. S7 are in agreement with the voltage plateaus for charge/discharge curves. There is a broad anodic peak at about 1.2 V, which is related to the reversible lithium reaction with Sn nanoparticles [49]. Meanwhile, a broad anodic peak at about 1.15 V might be attributed to the irreversible reaction of the electrode to form the solid electrolyte interface (SEI) layer on the surface of the electrode. Besides, obvious oxidation and reduction peaks at 0.1–0.2 V were

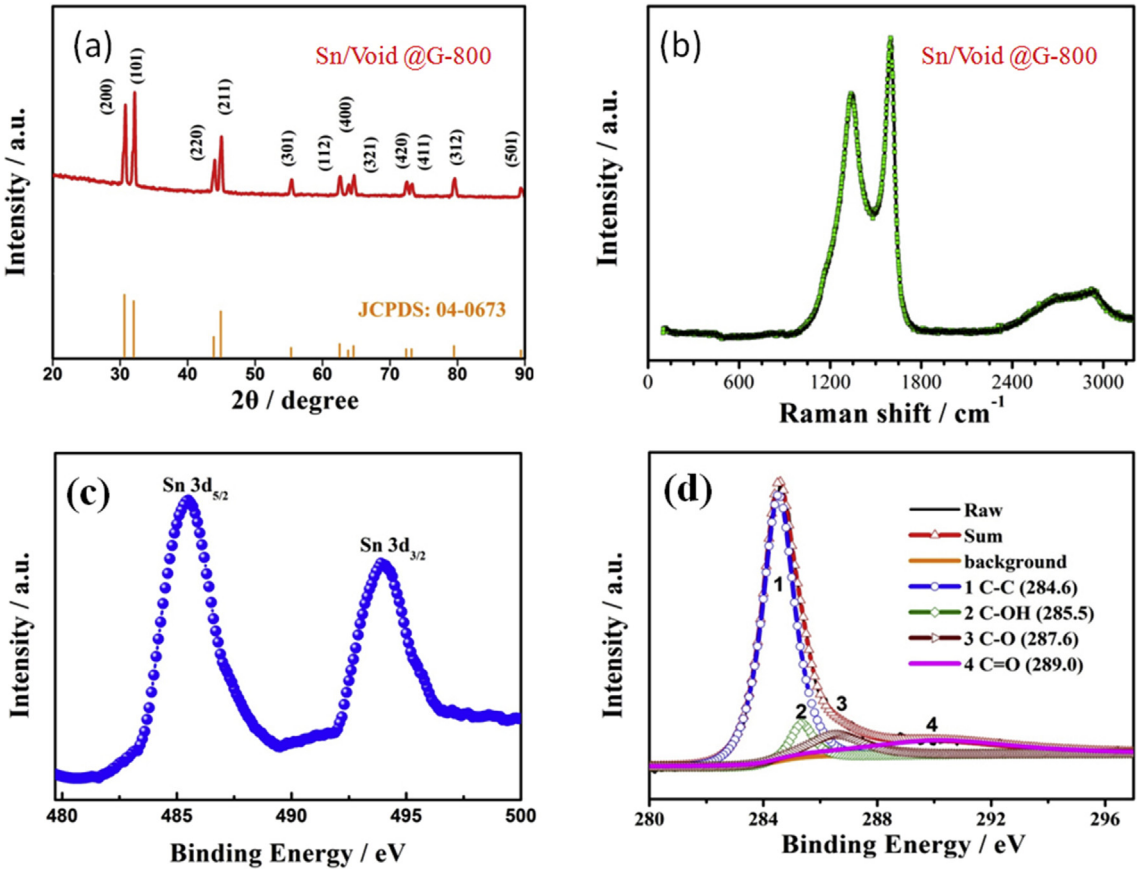

Fig. 3. (a) XRD pattern of Sn/Void@G-800 electrode materials; (b) Raman spectra of the Sn/Void @G-800 electrode materials; XPS spectrum of Sn/Void @G-800: (c, d) narrows scans of C1s and Sn3d, respectively.

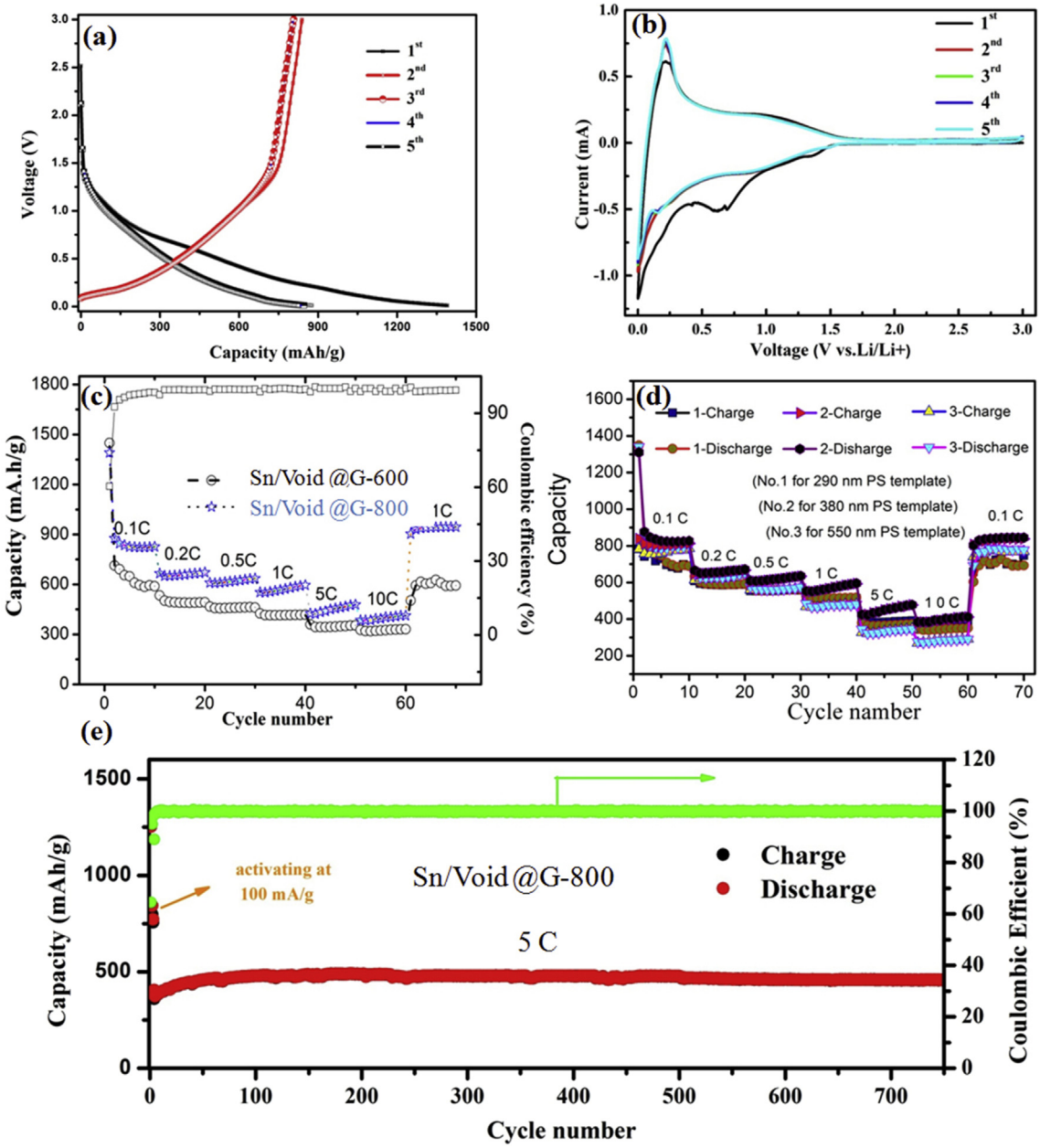

Fig. 4. (a) The first five cycle charge-discharge curves of the Sn/Void @G-800 an electrodes at 0.1C for LIBs; (b) CV curves of the Sn/Void @G-800 anode between 0.01 and 3.00 V (vs Li/Li^+) at a scan rate of 0.1 mV s^{-1}; (c) The multi-rate testing of the Sn/Void @G-800 and Sn/Void @G-600 electrodes at the charge-discharge current of various C rate, respectively; (d) The rate performance of the Sn/Void@G-800 with different size void; (e) Cycling performance of the Sn/Void @G-800 and Sn/Void @G-800 anode of LIBs, at a current of 0.5C rate.

also observed, which are attributed to the insertion/extraction of Li into/from graphene [50]. In addition, the cathodic peaks at 0.3–0.7 V can be associated with multistep electrochemical reduction reactions of the Li_xSn alloy. Fig. 4c shows the multi-rate performance of Sn/Void@G-800 electrode at various current densities. The Sn/Void@G-800 electrode shows a reversible specific capacity of 868.9, 654.9, 616.3, 566.4, 450.1, 393.5 mA h g^{-1} at 0.1, 0.2, 0.5, 1, 5 and 10C rates, respectively, which is better than that of the Sn/Void@G-600 electrode. When the C rate increases 100 times from 0.1 to 10C, the Sn/Void@G-800 anode shows high capacity retention ratio of 45.3%, revealing a good rate capacity. Besides, the electrochemical impedance spectra (EIS) studies further proved that the Sn/Void@G-800 electrode possesses the lower contact and charge-transfer resistances compared Sn/Void@G-600 electrode (see Fig. S8). For comparative experiments on the different scales of PS particles (290, 380, 550 nm) template was performed, and the micro-nano void of Sn/Void@G-800 electrode was tuned. Fig. 4d show that the size of void on surface of the Sn/Void@G-800 anode has obvious effect on the capacity and rate performance of samples, the Sn/Void@G-800 with medium sized void (~ 400 nm) have the best capacity and magnification properties, however, the initial coulomb efficiency increases as increase of size of the void. The cycling performances of the Sn/Void@G-800 electrodes with medium sized void are shown in Fig. 4e. The electrodes were first discharged/charged for three and five cycles to activating at 0.1C rate for electrode activation, then C rate was up to 5C and maintained for 700 cycles, and the reversible specific capacity shows almost no decaying. The Sn/Void@G-800 electrode displays

excellent cycling performance could be attributed to three reasons: (1) graphene possess elastic properties, which ensure the contact with Sn nanoparticles and protect the Li ion transport pathways in the charge-discharge cycle [51]; (2) graphene possess a larger surface area and the Sn nanoparticles uniformly doped in graphene-based 3D architecture could largely alleviate the destructive changes from large volume changes in the intercalation and deintercalation process of Li ion [52,53]; (3) after a heat treatment at high temperature, the electrical conductivity of Sn/Void@G is increased considerably, attributed to the reduction of GO, carbonization of the carbonaceous polymer, which could significantly reduce the loss [54,55]. For comparison, other reported Sn-based electrodes research works are summarized in Table S1, revealing the Sn/Void@G-800 anode possesses an excellent cycling performance.

The storage Na performances of the Sn/Void@G-800 electrodes with medium sized void were studied. As shown in Fig. 5a, the Sn/Void@G-800 anode displays a capacity of 1153 and 751 mAh g^{-1} in the first charge and discharge process with an initial coulombic efficiency of 65%. However, the Sn/Void @G-600 delivers initial coulombic efficiency of 35%, because low annealing temperature results in a low crystalline structure of graphene in Sn/Void@G-600 anode (see Fig. S9), which is proved by the TEM result. This BET result further proves that Sn/Void@G-800 have middle specific surface area (303.6 m^2/g) and mesoporous structures with a few nanometers have been observed (see Fig. s10). It is obvious that Sn/Void @G-800 anode exhibits high capacities at various rate testing (751 mAh g^{-1} vs 0.1C, 622 mAh g^{-1} vs 0.2C, 566 mAh g^{-1} vs 0.5C, 455 mAh g^{-1} vs 1C, 348 mAh g^{-1} vs 2C, 305 mAh g^{-1} vs 5C, 248 mAh g^{-1} vs 10C, 166 mAh g^{-1} vs 20C, respectively). This indicates the Sn/Void@G-800 anode may possess good structural stability during the charge/discharge process, leading to a better electrochemical performance at different current densities. More interestingly, the Sn/Void@G-800 anode can charge and discharge under 10C rate within several-minute time and simultaneously remain a high capacity of 240 mAh g^{-1}. The Sn/Void @G-800 anode displays a capacity of 350 mAh g^{-1} after 800 cycles, exhibiting excellent cycling stability (in Fig. 5d). The outstanding electrochemical storage Na performance of this new graphene-based composite electrode derives from its unique porous structure and tunable micro-nano void, which void as a highly efficient “bumper” to accommodate the large volume expansion of nano-Sn under charge and discharge process. The new type graphene based anode offers new opportunities for Na ion storage application of graphene composite in future.

4. Conclusions

In summary, the doped nano Sn 3D porous graphene structure were successfully fabricated by template method, and the tunable micro-nano void formed. The unique structure alleviates mechanical stress, accommodates volume variation, and ensures sufficient contact areas between the electrode and liquid electrolyte. With its use in an anode for LIBs, the discharge specific capacity still remains 45.3% of the as-prepared Sn/Void@G-800 electrode, when the C rate from 0.1C up to 5C. In addition, the Sn/Void @G-800 electrode

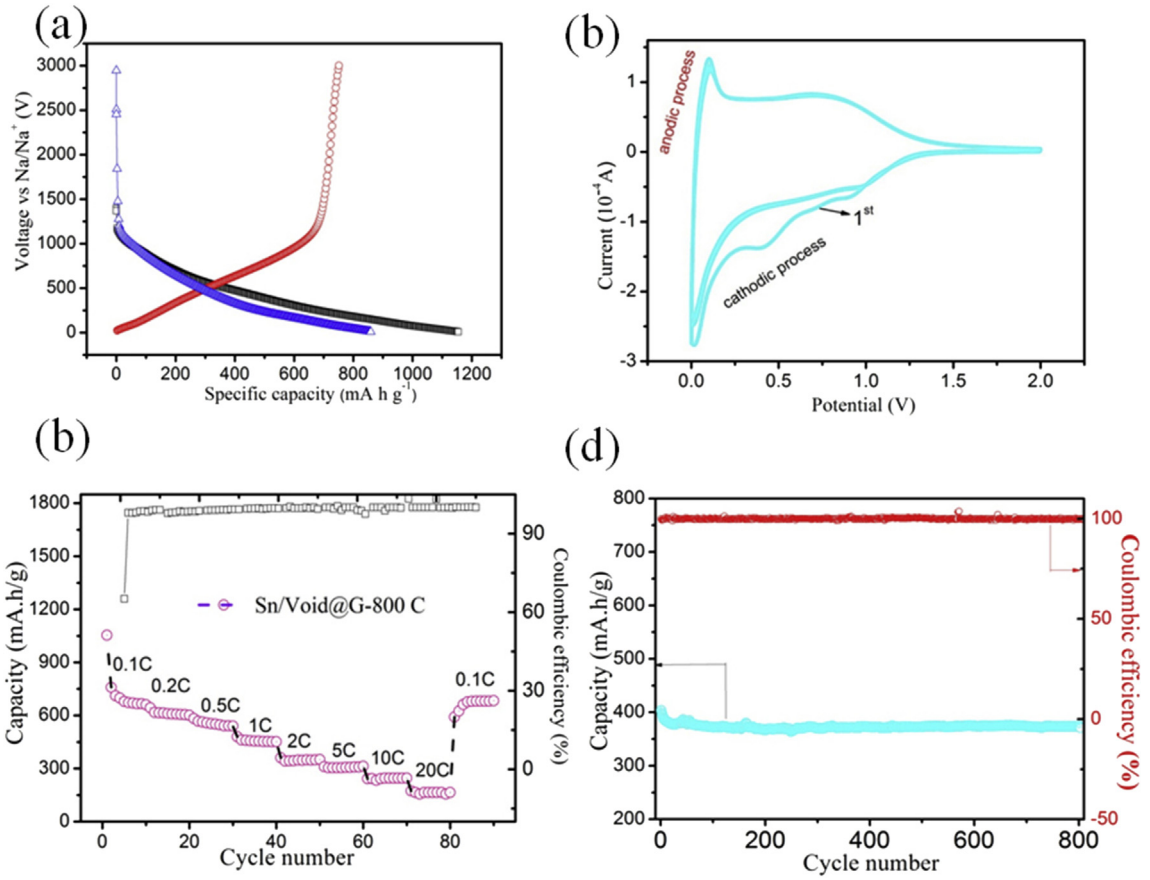

Fig. 5. (a) The fist charge-discharge curves of the Sn/Void @G-800 electrodes at 1 A g^{-1} for Na battery; (b) CV curves of the Sn/Void @G-800 anode between 0.01 and 3.00 V (vs Li/Li^+) at a scan rate of 0.1 mV s^{-1}; (c) The multi-rate testing of the Sn/Void@G-800 electrodes at the charge-discharge current of various C rate, respectively; (d) Cycling performance of the Sn/Void @G-800 anode of Na battery at a current of 2C rate.

shows excellent cycling stability with the first coulomb efficiency is 62.5%. The Sn/Void@G-800 electrode is also suitable for using as the anode for Na ion batteries and delivers an ultrahigh rate capability of more than 166 mAh g^{-1} at 20C and long-term cycling stability of 800 cycles at 2C. The outstanding electrochemical performance results from the uniform dispersion of Sn nanoparticles in the hierarchically porous graphene matrix with a buffered structure. The simplified synthesis approach and the well electrochemical performance of the Sn/Void@G electrode could be more beneficial to the large-scale application as the anode materials for an energy storage application.

Conflicts of interest

The authors declare that they have no conflict of interest.

Acknowledgements

The authors would like to acknowledge support from National Natural Science Foundation of China (Grant No.51761135123), the Natural Science Foundation of Heilongjiang Province of China (Grant No. E2016062), the China Postdoctoral Science Foundation (General Financial Grant No. 2018M630339), the Scientific Research Foundation for the Returned Overseas Chinese Scholars of the State Education Ministry (No. 20151098), Key Laboratory of Engineering Dielectrics and Its Application (Harbin University of Science and Technology) and Ministry of Education (Grant No. KF20171111).

Appendix A. Supplementary data

Supplementary data to this article can be found online at https://doi.org/10.1016/j.jallcom.2019.03.258.

References

[1] J.D. Liu, J.J. Liang, C.Y. Wang, J.M. Ma, Electrospun CoSe@N-doped carbon nanofibers with highly capacitive Li storage, J. Energy Chem. 33 (2019) 160–166.
[2] J.J. Liang, Z.X. Wei, C.Y. Wang, J.M. Ma, Vacancy-induced sodium-ion storage in N-doped carbon Nanofiber@MoS2 nanosheet arrays, Electrochim. Acta 285 (2018) 301–308.
[3] J.D. Huang, Z.X. Wei, J.Q. Liao, W. Ni, C.Y. Wang, J.M. Ma, Molybdenum and tungsten chalcogenides for lithium/sodium-ion batteries: beyond MoS2, J. Energy Chem. 33 (2019) 100–124.
[4] X. Zhang, X. Liu, C. Yang, N. Li, T. Ji, K. Yan, B. Zhu, J. Yin, J. Zhao, Y. Li, A V2O5-nanosheets-coated hard carbon fiber fabric as high-performance anode for sodium ion battery, Surf. Coat. Technol. 358 (2019) 661–666.
[5] M. Cao, M. Zhang, L. Xing, Q. Wang, X.-Y. Xue, One-step preparation of pomegranate-shaped Sn/SnO x/nanocarbon composites for fabricating ultrafast-charging/long-life lithium-ion battery, J. Alloys Compd. 694 (2017) 30–39.
[6] X.X. Liu, D.L. Chao, Y. Li, J. Hao, X.S. Liu, J.P. Zhao, J.Y. Lin, H.J. Fan, Z.X. Shen, A low-cost and one-step synthesis of N-doped monolithic quasi-graphene films with porous carbon frameworks for Li-ion batteries, Nano Energy 17 (2015) 43–51.
[7] D.L. Chao, P. Liang, Z. Chen, L.Y. Bai, H. Shen, X.X. Liu, X.H. Xia, Y.L. Zhao, S.V. Savilov, J.Y. Lin, Z.X. Shen, Pseudocapacitive Na-ion storage boosts high rate and areal capacity of self-branched 2D layered metal chalcogenide nanoarrays, ACS Nano 10 (2016) 10211–10219.
[8] S. Liu, Z. Tong, J. Zhao, X. Liu, J. Wang, X. Ma, C. Chi, Y. Yang, X. Liu, Y. Li, Rational selection of amorphous or crystalline V2O5 cathode for sodium-ion batteries, Phys. Chem. Chem. Phys. PCCP 18 (2016) 25645–25654.
[9] Y. Sun, S.X. Jin, G.W. Yang, J. Wang, C.X. Wang, Germanium nanowires-in-graphite tubes via self-catalyzed synergetic confined growth and shell-splitting enhanced Li-storage performance, ACS Nano 9 (2015) 3479–3490.
[10] A. Magasinski, P. Dixon, B. Hertzberg, A. Kvit, J. Ayala, G. Yushin, High-performance lithium-ion anodes using a hierarchical bottom-up approach, Nat. Mater. 9 (2010) 353–358.
[11] B. Luo, B. Wang, X.L. Li, Y.Y. Jia, M.H. Liang, L.J. Zhi, Graphene-confined Sn nanosheets with enhanced lithium storage capability, Adv. Mater. 24 (2012) 3538–3543.
[12] S.F. Yang, P.Y. Zavalij, M.S. Whittingham, Anodes for lithium batteries: tin revisited, Electrochem. Commun. 5 (2003) 587–590.
[13] M. Winter, J.O. Besenhard, Electrochemical lithiation of tin and tin-based intermetallics and composites, Electrochim. Acta 45 (1999) 31–50.
[14] J.Y. Huang, L. Zhong, C.M. Wang, J.P. Sullivan, W. Xu, L.Q. Zhang, S.X. Mao, N.S. Hudak, X.H. Liu, A. Subramanian, H.Y. Fan, L.A. Qi, A. Kushima, J. Li, In situ observation of the electrochemical lithiation of a single SnO2 nanowire electrode, Science 330 (2010) 1515–1520.
[15] J.M. Tarascon, M. Armand, Issues and challenges facing rechargeable lithium batteries, Nature 414 (2001) 359–367.
[16] B. Wang, B. Luo, X.L. Li, L.J. Zhi, The dimensionality of Sn anodes in Li-ion batteries, Mater. Today 15 (2012) 544–552.
[17] A.R. Kamali, D.J. Fray, Tin-based materials as advanced anode materials for lithium ion batteries: a review, Rev. Adv. Mater. Sci. 27 (2011) 14–24.
[18] J.S. Chen, X.W. Lou, SnO2 and TiO2 nanosheets for lithium-ion batteries, Mater. Today 15 (2012) 246–254.
[19] J. Hassoun, G. Derrien, S. Panero, B. Scrosati, A nanostructured Sn-C composite lithium battery electrode with unique stability and high electrochemical performance, Adv. Mater. 20 (2008) 3169–3175.
[20] J. Hwang, S.H. Woo, J. Shim, C. Jo, K.T. Lee, J. Lee, One-Pot synthesis of tin-embedded carbon/silica nanocomposites for anode materials in lithium-ion batteries, ACS Nano 7 (2013) 1036–1044.
[21] G. Wang, Y.Q. Ma, Z.Y. Liu, J.N. Wu, Novel highly porous Sn-C composite as high performance anode material for lithium-ion batteries, Electrochim. Acta 65 (2012) 275–279.
[22] Y. Liu, J. Yin, X. Liu, X. Zhao, M. Chen, J. Li, H. Zhao, C. Zhu, B. Su, Fabrication of polymer composite films with carbon composite nanofibers doped MWNTs-OH for multilevel memory device application, Compos. B Eng. 156 (2019) 252–258.
[23] B. Zhu, X. Liu, N. Li, C. Yang, T. Ji, K. Yan, H. Chi, X. Zhang, F. Sun, D. Sun, C. Chi, X. Wang, Y. Wang, L. Chen, L. Yao, Three-dimensional porous graphene microsphere for high-performance anode of lithium ion batteries, Surf. Coat. Technol. 360 (2019) 232–237.
[24] H. Liu, X.J. Chen, L. Deng, X. Su, K. Guo, Z.F. Zhu, Preparation of ultrathin 2D MoS2/graphene heterostructure assembled foam-like structure with enhanced electrochemical performance for lithium-ion batteries, Electrochim. Acta 206 (2016) 184–191.
[25] Y. Wang, X. Liu, C. Yang, N. Li, K. Yan, T. Ji, H. Chi, F. Sun, J. Zhao, Y. Li, Low cost fabrication of three-dimensional hierarchical porous graphene anode material for sodium ion batteries application, Surf. Coat. Technol. 360 (2019) 110–115.
[26] P. Zheng, T. Liu, S.W. Guo, Micro-nano structure hard carbon as a high performance anode material for sodium-ion batteries, Sci. Rep.-Uk 6 (2016) 35620.
[27] P. Zheng, T. Liu, J.Z. Zhang, L.F. Zhang, Y. Liu, J.F. Huang, S.W. Guo, Sweet potato-derived carbon nanoparticles as anode for lithium ion battery, RSC Adv. 5 (2015) 40737–40741.
[28] L.Y. Cao, W.L. Hui, Z.W. Xu, J.F. Huang, P. Zheng, J.Y. Li, Q.Q. Sun, Rape seed shuck derived-lamellar hard carbon as anodes for sodium-ion batteries, J. Alloys Compd. 695 (2017) 632–637.
[29] H.W. Wu, Y. Huang, W.C. Zhang, X. Sun, Y.W. Yang, L. Wang, M. Zong, Lock of sulfur with carbon black and a three-dimensional graphene@carbon nanotubes coated separator for lithium-sulfur batteries, J. Alloys Compd. 708 (2017) 743–750.
[30] P. Zheng, T. Liu, X.Y. Yuan, L.F. Zhang, Y. Liu, J.F. Huang, S.W. Guo, Enhanced performance by enlarged nano-pores of holly leaf-derived lamellar carbon for sodium-ion battery anode, Sci. Rep.-Uk 6 (2016).
[31] J. Fei, Y.L. Cui, J.Y. Li, Z.W. Xu, J. Yang, R.Y. Wang, Y.Y. Cheng, J.F. Hang, A flexible Sb2O3/carbon cloth composite as a free-standing high performance anode for sodium ion batteries, Chem. Commun. 53 (2017) 13165–13167.
[32] K.X. Wang, Q.C. Zhu, J.S. Chen, Strategies toward high-performance cathode materials for lithium-oxygen batteries, Small 14 (2018).
[33] X. Liu, Y. Li, W. Guo, X. Sun, Y. Feng, D. Sun, Y. Liu, K. Yan, Z. Wu, B. Su, J. Yin, Dielectric and mechanical properties of polyimide composite films reinforced with graphene nanoribbon, Surf. Coat. Technol. 320 (2017) 497–502.
[34] A. Marcinek, L.J. Hardwick, T.J. Richardson, X. Song, R. Kostecki, Microwave plasma chemical vapor deposition of nano-structured Sn/C composite thin-film anodes for Li-ion batteries, J. Power Sources 173 (2007) 965–971.
[35] L.Z. Zhao, S.J. Hu, Q. Ru, W.S. Li, X.H. Hou, R.H. Zeng, D.S. Lu, Effects of graphite on electrochemical performance of Sn/C composite thin film anodes, J. Power Sources 184 (2008) 481–484.
[36] J.W. Zheng, S.M.L. Nai, M.F. Ng, P. Wu, J. Wei, M. Gupta, DFT study on nano structures of Sn/CNT complex for potential Li-ion battery application, J. Phys. Chem. C 113 (2009) 14015–14019.
[37] Y.H. Yu, Q. Yang, D.H. Teng, X.P. Yang, S. Ryu, Reticular Sn nanoparticle-dispersed PAN-based carbon nanofibers for anode material in rechargeable lithium-ion batteries, Electrochem. Commun. 12 (2010) 1187–1190.
[38] F.R. Beck, R. Epur, D.H. Hong, A. Manivannan, P.N. Kumta, Microwave derived facile approach to Sn/graphene composite anodes for, lithium-ion batteries, Electrochim. Acta 127 (2014) 299–306.
[39] S.K. Liu, X.S. Liu, J.P. Zhao, Z.Q. Tong, J. Wang, X.X. Ma, C.X. Chi, D.P. Su, X.X. Liu, Y. Li, Three dimensional hierarchically porous crystalline MnO2 structure design for a high rate performance lithium-ion battery anode, RSC Adv. 6 (2016) 85222–85229.
[40] J.-l. Li, J.-h. Yin, T. Ji, Y. Feng, Y.-y. Liu, H. Zhao, Y.-p. Li, C.-c. Zhu, D. Yue, B. Su, X.-x. Liu, Microstructure evolution effect on high-temperature thermal conductivity of LDPE/BNNS investigated by in-situ SAXS, Mater. Lett. 234 (2019) 74–78.
[41] H.L. Wang, J.T. Robinson, X.L. Li, H.J. Dai, Solvothermal reduction of chemically

exfoliated graphene sheets, J. Am. Chem. Soc. 131 (2009) 9910–9911.
[42] A.C. Ferrari, J. Robertson, Interpretation of Raman spectra of disordered and amorphous carbon, Phys. Rev. B 61 (2000) 14095–14107.
[43] X. Liu, D. Chao, D. Su, S. Liu, L. Chen, C. Chi, J. Lin, Z.X. Shen, J. Zhao, L. Mai, Y. Li, Graphene nanowires anchored to 3D graphene foam via self-assembly for high performance Li and Na ion storage, Nano Energy 37 (2017) 108–117.
[44] C.D. Wang, Y. Li, Y.S. Chui, Q.H. Wu, X.F. Chen, W.J. Zhang, Three-dimensional Sn-graphene anode for high-performance lithium-ion batteries, Nanoscale 5 (2013) 10599–10604.
[45] Z.H. Wen, S.M. Cui, H.J. Kim, S. Mao, K.H. Yu, G.H. Lu, H.H. Pu, O. Mao, J.H. Chen, Binding Sn-based nanoparticles on graphene as the anode of rechargeable lithium-ion batteries, J. Mater. Chem. 22 (2012) 3300–3306.
[46] Z. Tan, Z.H. Sun, H.H. Wang, Q. Guo, D.S. Su, Fabrication of porous Sn-C composites with high initial coulomb efficiency and good cyclic performance for lithium ion batteries, J. Mater. Chem. A 1 (2013) 9462–9468.
[47] X.Y. Zhou, Y.L. Zou, J. Yang, Periodic structures of Sn self-inserted between graphene interlayers as anodes for Li-ion battery, J. Power Sources 253 (2014) 287–293.
[48] A. Palinkas, G. Molnar, G.Z. Magda, C.Y. Hwang, L. Tapaszto, P. Samuely, P. Szabo, Z. Osvath, Novel graphene/Sn and graphene/SnOx hybrid nanostructures: induced superconductivity and band gaps revealed by scanning probe measurements, Carbon 124 (2017) 611–617.
[49] R. Demir-Cakan, Y.S. Hu, M. Antonietti, J. Maier, M.M. Titirici, Facile one-pot synthesis of mesoporous SnO2 microspheres via nanoparticles assembly and lithium storage properties, Chem. Mater. 20 (2008) 1227–1229.
[50] L.Y. Beaulieu, K.C. Hewitt, R.L. Turner, A. Bonakdarpour, A.A. Abdo, L. Christensen, K.W. Eberman, J.L. Krause, J.R. Dahn, The electrochemical reaction of Li with amorphous Si-Sn alloys, J. Electrochem. Soc. 150 (2003) A149–A156.
[51] J. Yue, X. Gu, X.L. Jiang, L. Chen, N.N. Wang, J. Yang, X.J. Ma, Coaxial manganese dioxide@N-doped carbon nanotubes as superior anodes for lithium ion batteries, Electrochim. Acta 182 (2015) 676–681.
[52] Y.M. Li, X.J. Lv, J. Lu, J.H. Li, Preparation of SnO2-nanocrystal/graphene-nanosheets composites and their lithium storage ability, J. Phys. Chem. C 114 (2010) 21770–21774.
[53] S.M. Paek, E. Yoo, I. Honma, Enhanced cyclic performance and lithium storage capacity of SnO2/graphene nanoporous electrodes with three-dimensionally delaminated flexible structure, Nano Lett. 9 (2009) 72–75.
[54] J. Fan, T. Wang, C.Z. Yu, B. Tu, Z.Y. Jiang, D.Y. Zhao, Ordered, nanostructured tin-based oxides/carbon composite as the negative-electrode material for lithium-ion batteries, Adv. Mater. 16 (2004) 1432–1437.
[55] J. Yao, X.P. Shen, B. Wang, H.K. Liu, G.X. Wang, In situ chemical synthesis of SnO2-graphene nanocomposite as anode materials for lithium-ion batteries, Electrochem. Commun. 11 (2009) 1849–1852.